PERGAMON

International Journal of Solids and Structures 40 (2003) 2195–2213

INTERNATIONAL JOURNAL OF SOLIDS and STRUCTURES

www.elsevier.com/locate/ijsolstr

Identification of orthotropic damages within a thin uniform plate

Usik Lee *, Kyoungkeun Cho, Jinho Shin

Department of Mechanical Engineering, Inha University, 253 Yonghyun-Dong, Nam-Ku, Inchon 402-751, South Korea

Received 28 February 2002; received in revised form 6 January 2003

Abstract

The line crack-like damage generated within a small material volume may change the material behavior of the material volume from initially isotropic to effectively orthotropic, depending on damage orientation. Thus, the change in material behavior can be used to identify the orientation of line crack-like damage with respect to the reference coordinates. Motivated from this observation, first the equation of motion is derived for the thin uniform plate with line crack-like local damages. The locations and severities of damages are characterized by using a damage distribution function, and a damaged small material volume is represented by the effective orthotropic elastic stiffnesses, which are derived in terms of damage orientation and size. Next, a new damage identification theory is developed to identify the orientations of local damages, in addition to their locations and severities, by using the frequency response functions measured from the damaged plate. Finally, the effects of damage orientation on the vibration responses of a plate are numerically investigated, and the numerically simulated damage identification tests are conducted to verify the present damage identification theory.

Keywords: Structural damage; Orthotropic damage; Damage identification; Thin plate; Vibration; Frequency response function; Damage orientation; Continuum damage model

1. Introduction

Existence of structural damages within a structure leads to the changes in dynamic characteristics of the structure such as the vibration responses, natural frequencies, mode shapes, and the modal dampings. Therefore, the changes in dynamic characteristics of a structure can be used in turn to detect, locate and quantify the structural damages generated within the structure. In the literature, a variety of structural damage identification methods (SDIMs), including the finite element model (FEM) update techniques and the experimental-data-based methods, have appeared over the years.

The FEM update techniques (e.g., Kabe, 1985; Zimmermann and Kaouk, 1994; Lim, 1995) have a drawback because it requires reducing the degrees of freedom or extending the measured modal parameters,

* Corresponding author. Tel.: +82-32-860-7318; fax: +82-32-866-1434.
E-mail address: ulee@inha.ac.kr (U. Lee).

0020-7683/03/$ - see front matter © 2003 Elsevier Science Ltd. All rights reserved.
doi:10.1016/S0020-7683(03)00055-6

which may result in the loss of physical interpretability and the errors due to the stiffness diffusion that smears the damage-induced localized changes in stiffness matrix into the entire stiffness matrix. Thus, various experimental-data-based SDIMs have been proposed in the literature as the alternatives to the FEM-update techniques. The existing experimental-data-based SDIM can be classified into several groups depending on the type of experimental data used to detect, locate, and/or quantify structural damages. They include the changes in modal data (e.g., Adams et al., 1978; Luo and Hanagud, 1997; Bicanic and Chen, 1997; Hassiotis, 2000), frequency response functions (FRF) (e.g., Wang et al., 1997; Thyagarajan et al., 1998; Lee and Shin, 2002a,b), strain energy (e.g., Cornwell et al., 1999), transfer function parameters (e.g., Lew, 1995), flexibility matrix (e.g., Pandey and Biswas, 1995), residual forces (e.g., Ricles and Kosmatka, 1992; Castello et al., 2002), mechanical impedances (e.g., Cawley, 1984), and so forth. It is interesting to find that most of experimental-data-based SDIMs in the literature have been derived from FEM model-based eigenvalue problems and that they have been applied mostly to one-dimensional structures such as beams, frame structures, and truss structures.

Though there have been many studies on the vibration of cracked plates (e.g., Lynn and Kumbasar, 1967; Lee and Lim, 1993; Dimarogonas, 1996; Lee and Kim, 2001), there have been only a small number of studies on the identification of damages within the plates. In the literature, Cawley and Adams (1979) are the first who locates the defects within a rectangular plate by using natural frequency changes only. Araujo dos Santos et al. (2000) used both natural frequencies and vibration modes to detect the damages within a laminated rectangular plate, and Chen and Bicanic (2000) introduced a method in which the incomplete natural frequencies and vibration modes can be used to detect the damages within a cantilever plate. The damage detection methods by Cawley and Adams (1979), Araujo dos Santos et al. (2000), and Chen and Bicanic (2000) are all derived from FEM model-based eigenvalue problems. Khadem and Rezaee (2000) introduced an analytical approach in which the changes in natural frequencies are used for obtaining the location and depth of a crack on the in-plane loaded plate. Later, Lee et al. (2001) developed an SDIM in which the FRF measured from a damaged plate is used for identifying the locations and severities of many local damages at a time.

The failure of most structural members involves general degradation of elastic properties due to the localized nucleation and growth of damages (i.e., voids, cavities, or cracks of the size of crystal grains) and their ultimate coalescences into the larger and larger size of material fracture. This implies that the orientation of local damages may control the direction of crack propagation within a structure member. Because the damage orientation will play a very important role to determine the failure pattern and remaining life of a structure member, it is mandatory to develop an SDIM that is capable of identifying the orientations of local damages, together with their locations and severities. However, to the authors' best knowledge, the main concerns of the previous experimental-data-based SDIMs existing in the literature are mostly confined to locate and quantify local damages within a structure, without showing the capability to identify the orientations of local damages. Motivated from this observation, this paper introduces a new SDIM by which the orientations of local damages within a thin uniform plate, in addition to their locations and severities, can be simultaneously identified.

The surfaces of material fracture can be considered as the continual propagation and coalescence of film-like small local cracks. Thus, it may be pertinent to consider a local damage, which is film-like and uniform through the plate thickness, as the equivalent line through-crack (simply, line crack). Based on the continuum damage mechanics, Lee et al. (1997) showed that a small material volume (SMV) with a line crack behaves *effectively* orthotropic (i.e., orthotropic damage), while an SMV with a circular crack behaves *effectively* isotropic (i.e., isotropic damage). They represented the material behavior of the SMV with a line crack in terms of the *effective* orthotropic elastic stiffnesses, which are the functions of the isotropic elastic stiffnesses, crack orientation, and the size of line crack (Lee et al., 1997). Thus, the changes in local elastic stiffnesses from initially isotropic to *effectively* orthotropic can be considered as the indicator of current crack orientation: this observation brings a new SDIM developed in the present study.

Thus, the purposes of the present study are: (1) to derive the equation of motion for the thin uniform rectangular plate with line crack-like damages by using a continuum damage representation, and (2) to develop a new SDIM by which the orientations of local damages, in addition to their locations and severities, can be identified at a time.

2. Effective orthotropic damage representation

Consider an elastic thin rectangular plate with the thickness h and the widths L_x and L_y in the x- and y-directions, respectively. The intact plate material is isotropic and has Young's modulus E and Poisson's ratio v. Assume there is a line crack of length $2l$, centered at (x_D, y_D) and aligned with the crack coordinate '1' which is oriented $\theta°$ with respect to the global coordinate x, as shown in Fig. 1(a). In the following, the crack coordinates will be represented by the subscripts 1 and 2, if not mentioned otherwise.

Lee et al. (1997) showed that the *effective* elastic stiffnesses Q_{ij}^D for the SMV containing a line crack-like damage could be derived as follows:

$$Q_{ij}^D = Q_{ij}(1 - e_{ij}\mathscr{D}) \quad (i,j = 1,2,6; \text{no sum}) \tag{1}$$

where Q_{ij} are the reduced stiffnesses for the intact isotropic material under the plane stress state (Whitney, 1996) and e_{ij} are the *effective* material directivity parameters given by

$$\begin{aligned} &e_{11} = \frac{2v^2}{1-v^2}, \quad e_{22} = e_{12} = e_{21} = \frac{2}{1-v^2} \\ &e_{16} = e_{26} = e_{61} = e_{62} = 0, \quad e_{66} = \frac{2}{1+v} \end{aligned} \tag{2}$$

For the case of isotropic damage such as the circular through-crack (i.e., circular hole), the values of e_{ij} are given by

$$e_{11} = e_{22} = e_{12} = e_{21} = e_{66} = 1, \quad e_{16} = e_{26} = e_{61} = e_{62} = 0 \tag{3}$$

In Eq. (1), $\mathscr{D}$ is the damage variable defined by the ratio of the volume of the SMV (i.e., $4\overline{xy}h$) containing a single line crack inside and the effective damaged volume (i.e., πhl^2) determined by the size of crack (Lee et al., 1997). Thus, $\mathscr{D}$ represents the averaged severity of damage within an SMV, which is called herein the *effective* damage magnitude. The *effective* damage magnitude $0 \leqslant \mathscr{D} \leqslant 1$ may have two extreme values as

$$\mathscr{D} = \frac{\pi hl^2}{4\overline{xy}h} = \begin{cases} 0 & \text{for intact state} \\ 1 & \text{for complete material failure} \end{cases} \tag{4}$$

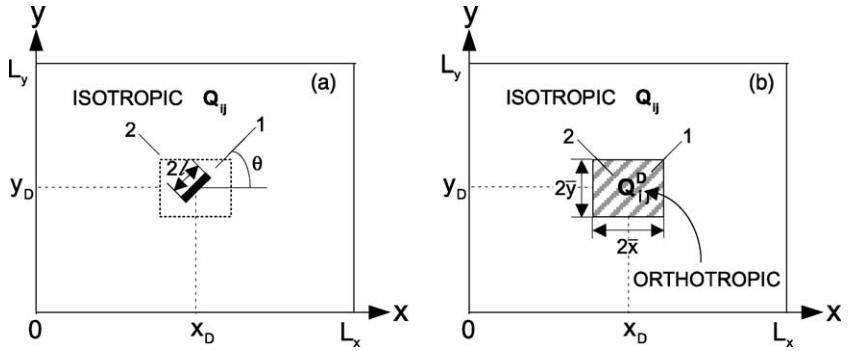

Fig. 1. (a) Initially isotropic rectangular plate with a line through-crack and (b) its equivalent continuum damage representation in terms of effective orthotropic elastic stiffnesses.

Note that the effective orthotropic elastic stiffnesses Q_{ij}^D given by Eq. (1) are all measured with respect to the crack coordinates 1 and 2. Thus, the effective elastic stiffness with respect to the global coordinates x and y can be obtained by using the coordinates transformation as follows:

$$\overline{\boldsymbol{Q}} = \boldsymbol{T}(\theta)^{\mathrm{T}} \boldsymbol{Q}^D \boldsymbol{T}(\theta) \tag{5}$$

where $\boldsymbol{T}(\theta)$ is the coordinates transformation matrix (Whitney, 1996), in which θ denotes the crack orientation (degrees) with respect to the global coordinate x. The superscript 'T' denotes the transpose of matrix.

In the following, the SMV containing a line crack-like damage (simply, damage) will be represented in terms of the effective elastic stiffnesses of Eq. (5) ($\overline{Q}_{ij}$) that are determined from the reduced stiffness of intact isotropic solid (Q_{ij}), the effective material directivity parameters (e_{ij}), the damage orientation (θ), and the damage variable ($\mathscr{D}$).

3. Dynamics of a plate with orthotropic damages

3.1. Equation of motion

For small amplitude vibration, the equation of motion for a thin uniform plate is given by (Whitney, 1996)

$$\frac{\partial^2 M_x}{\partial x^2} + 2\frac{\partial^2 M_{xy}}{\partial x \partial y} + \frac{\partial^2 M_y}{\partial y^2} + f(x,y,t) = \rho A \ddot{w} \tag{6}$$

where $w(x,y,t)$ is the flexural deflection, $f(x,y,t)$ the external force applied normal to the surface of plate, ρA is the mass density per area, and dot $(\cdot)$ denotes the partial derivative with respect to time t. The moment resultants M_x, M_y, and M_{xy} are defined by

$$\begin{Bmatrix} M_x \\ M_y \\ M_{xy} \end{Bmatrix} = \begin{bmatrix} \overline{D}_{11} & \overline{D}_{12} & \overline{D}_{16} \\ & \overline{D}_{22} & \overline{D}_{26} \\ \text{symm} & & \overline{D}_{66} \end{bmatrix} \begin{Bmatrix} \kappa_{xx} \\ \kappa_{yy} \\ \kappa_{xy} \end{Bmatrix} \tag{7}$$

where κ_{ij} are the curvatures and $\overline{D}_{ij}$ are the bending stiffnesses related to the transformed plane-stress reduced stiffnesses $\overline{Q}_{ij}$ as follows (Whitney, 1996):

$$\overline{D}_{ij} = \frac{h^3}{12}\overline{Q}_{ij} \quad (i,j = 1,2,6) \tag{8}$$

Because the plate shown in Fig. 1(b) consists of the intact zone (outside SMV, isotropic) and the damaged zone (inside SMV, effectively orthotropic), $\overline{D}_{ij}$ have the values as follows:

$$\overline{D}_{ij} = \begin{cases} D_{ij} = \overline{D}_{ij}(\mathscr{D} = 0) & \text{(outside SMV)} \\ D_{ij}^D = \overline{D}_{ij}(\mathscr{D}) & \text{(inside SMV)} \end{cases} \quad (i,j = 1,2,6) \tag{9}$$

The intact plate bending stiffnesses D_{ij} for the outside of SMV are given by

$$\begin{aligned} &D_{11} = D_{22} = D, \quad D_{12} = D_{21} = vD \\ &D_{16} = D_{61} = D_{26} = D_{62} = 0, \quad D_{66} = \left(\frac{1-v}{2}\right)D \end{aligned} \tag{10}$$

where D is the flexural rigidity of plate defined by

$$D = \frac{Eh^3}{12(1-v^2)} \tag{11}$$

Based on Eq. (9), the bending stiffnesses all over the plate can be represented by

$$\overline{D}_{ij}(x,y) = D_{ij} - \Delta D_{ij} d(x,y) \quad (i,j = 1,2,6) \tag{12}$$

where

$$\Delta D_{ij} = D_{ij} - D_{ij}^{D} \quad (i,j = 1,2,6) \tag{13}$$

and

$$d(x,y) = [H(x_D - \bar{x}) - H(x_D + \bar{x})] \times [H(y_D - \bar{y}) - H(y_D + \bar{y})] \tag{14}$$

The perturbed plate bending stiffnesses ΔD_{ij} represent the *effective* degradation of the plate bending stiffnesses due to the existence of damage. The damage distribution function $d(x,y)$ plays the roll of locating and quantifying the severity of damage on the plate. In Eq. (14), $H(x)$ and $H(y)$ are the Heaviside's unit functions defined by

$$H(a) = \begin{cases} 1 & \text{when } x > a \quad (\text{or } y > a) \\ 0 & \text{when } x < a \quad (\text{or } y > a) \end{cases} \tag{15}$$

Substituting Eq. (12) into Eq. (7) and the result into Eq. (6) yields the equation of motion for the plate with a line crack as follows:

$$D\nabla^4 w - \left(\frac{\partial^2 \phi_1}{\partial x^2} + \frac{\partial^2 \phi_2}{\partial y^2} + \frac{\partial^2 \phi_3}{\partial x \partial y} \right) + \rho A \ddot{w} = f(x,y,t) \tag{16}$$

where

$$\begin{aligned} \phi_1 &= d(x,y) \left[\Delta D_{11} \frac{\partial^2 w}{\partial x^2} + \Delta D_{12} \frac{\partial^2 w}{\partial y^2} + 2\Delta D_{16} \frac{\partial^2 w}{\partial x \partial y} \right] \\ \phi_2 &= d(x,y) \left[\Delta D_{12} \frac{\partial^2 w}{\partial x^2} + \Delta D_{22} \frac{\partial^2 w}{\partial y^2} + 2\Delta D_{26} \frac{\partial^2 w}{\partial x \partial y} \right] \\ \phi_3 &= d(x,y) \left[2\Delta D_{16} \frac{\partial^2 w}{\partial x^2} + 2\Delta D_{26} \frac{\partial^2 w}{\partial y^2} + 4\Delta D_{66} \frac{\partial^2 w}{\partial x \partial y} \right] \end{aligned} \tag{17}$$

where ∇^4 denotes the biharmonic operator. For the intact plate, the second term in the left-hand side of Eq. (16) completely vanishes. Though Eq. (16) is derived for a single damage, it can be readily generalized for many line cracks by modifying Eq. (14) to encompass all local damages.

3.2. Dynamic responses

The forced vibration response of a thin uniform plate with a single damage can be assumed as

$$w(x,y,t) = \sum_{m=1}^{M} W_m(x,y) q_m(t) \tag{18}$$

where $q_m(t)$ are the modal coordinates, and $W_m(x,y)$ are the natural modes of intact plate satisfying the eigenvalue problem

$$D\nabla^4 W_m = \rho A \Omega_m^2 W_m \quad (\text{no sum on } m) \tag{19}$$

and the orthogonality property

$$\int \int \rho A W_m W_n \, \mathrm{d}x \, \mathrm{d}y = \delta_{mn}$$

$$\int\int DW_m\nabla^4 W_n\,\mathrm{d}x\,\mathrm{d}y = \Omega_m^2\delta_{mn} \quad \text{(no sum on } m\text{)} \tag{20}$$

where Ω_m are the natural frequencies of the intact plate, and δ_{mn} denotes the Kronecker delta. The natural modes $W_m(x,y)$ used in Eq. (18) can be analytically obtained in the closed forms for Levy-type plates (Reddy, 1999). However, for the non-Levy-type plates, the numerical approach such as the finite element method can be applied to obtain the natural modes.

Substituting Eq. (18) into Eq. (16) and then applying Eq. (20) yields the modal equations as follows:

$$\ddot{\boldsymbol{q}} + \mathrm{diag}[\Omega^2]\boldsymbol{q} - \lambda\boldsymbol{q} = \boldsymbol{f}(t) \tag{21}$$

where

$$\boldsymbol{q} = \{\, q_1 \quad q_2 \quad \dots \quad q_M \,\}^{\mathrm{T}}, \quad \mathrm{diag}[\Omega^2] = \begin{bmatrix} \ddots & & \\ & \Omega_m^2 & \\ & & \ddots \end{bmatrix} \tag{22}$$

and $\boldsymbol{f}$ is the nodal forces vector computed from

$$f_m(t) = \int_0^{L_y}\int_0^{L_x} f(x,y,t)W_m(x,y)\,\mathrm{d}x\,\mathrm{d}y \tag{23}$$

and the matrix $\boldsymbol{\lambda}$ is computed from

$$\lambda_{mn} = \int_{y_D-\bar{y}}^{y_D+\bar{y}}\int_{x_D-\bar{x}}^{x_D+\bar{x}} \boldsymbol{\Phi}_{mn}(x,y)\boldsymbol{\Delta}d(x,y)\,\mathrm{d}x\,\mathrm{d}y \tag{24}$$

where $\boldsymbol{\Phi}_{mn}$ is the (one by six) matrix defined by

$$\begin{aligned}\boldsymbol{\Phi}_{mn}(x,y) = \Bigg[&\frac{\partial^2 W_m}{\partial x^2}\frac{\partial^2 W_n}{\partial x^2}, \frac{\partial^2 W_m}{\partial x^2}\frac{\partial^2 W_n}{\partial y^2} + \frac{\partial^2 W_n}{\partial x^2}\frac{\partial^2 W_m}{\partial y^2}, 2\left(\frac{\partial^2 W_m}{\partial x^2}\frac{\partial^2 W_n}{\partial x\partial y} + \frac{\partial^2 W_n}{\partial x^2}\frac{\partial^2 W_m}{\partial x\partial y}\right),\\ &\frac{\partial^2 W_m}{\partial y^2}\frac{\partial^2 W_n}{\partial y^2}, 2\left(\frac{\partial^2 W_m}{\partial y^2}\frac{\partial^2 W_n}{\partial x\partial y} + \frac{\partial^2 W_n}{\partial y^2}\frac{\partial^2 W_m}{\partial x\partial y}\right), 4\frac{\partial^2 W_m}{\partial x\partial y}\frac{\partial^2 W_n}{\partial x\partial y}\Bigg]\end{aligned} \tag{25}$$

and $\boldsymbol{\Delta}$ is the (six by one) vector defined by

$$\boldsymbol{\Delta} = \{\Delta D_{11}, \Delta D_{12}, \Delta D_{16}, \Delta D_{22}, \Delta D_{26}, \Delta D_{66}\}^{\mathrm{T}} \tag{26}$$

The symmetric matrix $\boldsymbol{\lambda}$ reflects the influence of damage and it is called 'damage influence matrix' (Lee and Shin, 2002a). The off-diagonal terms of $\boldsymbol{\lambda}$ induce the coupling between modal coordinates.

By using Eqs. (5), (8)–(10), Eq. (13) can be expressed as

$$\Delta D_{ij} = Z_{ij}(\theta)\mathscr{D} \quad (i,j = 1,2,6) \tag{27}$$

where Z_{ij} are computed from

$$\boldsymbol{Z}(\theta) = \frac{h^3}{12}\boldsymbol{T}(\theta)^{\mathrm{T}}\boldsymbol{E}\boldsymbol{T}(\theta) \tag{28}$$

where $\boldsymbol{T}$ is the coordinates transformation matrix defined in Eq. (5), and $\boldsymbol{E}$ is the matrix computed from

$$E_{ij} = Q_{ij}e_{ij} \quad (i,j = 1,2,6; \text{no sum}) \tag{29}$$

The values of e_{ij} are given by Eq. (2) for orthotropic damages and by Eq. (3) for isotropic damages. Substituting Eq. (27) into Eq. (26) gives

$$\Delta = D(\boldsymbol{P} + \boldsymbol{H}_c + \boldsymbol{H}_s)\mathscr{D} \tag{30}$$

where $\boldsymbol{P}$, $\boldsymbol{H}_c$, and $\boldsymbol{H}_s$ are the vectors defined, for orthotropic damage, by

$$\begin{aligned}\boldsymbol{P} &= \left\{ \frac{1+\nu^2}{1-\nu^2} \quad \frac{2\nu}{1-\nu^2} \quad 0 \quad \frac{1+\nu^2}{1-\nu^2} \quad 0 \quad \frac{1-\nu}{2(1+\nu)} \right\}^{\mathrm{T}} \\ \boldsymbol{H}_c &= \{ -\cos 2\theta \quad 0 \quad 0 \quad \cos 2\theta \quad 0 \quad 0 \}^{\mathrm{T}} \\ \boldsymbol{H}_s &= \{ 0 \quad 0 \quad -\sin 2\theta \quad 0 \quad -\sin 2\theta \quad 0 \}^{\mathrm{T}}\end{aligned} \tag{31}$$

and, for isotropic damage, by

$$\begin{aligned}\boldsymbol{P} &= \{ 1 \quad \nu \quad 0 \quad 1 \quad 0 \quad (1-\nu)/2 \}^{\mathrm{T}} \\ \boldsymbol{H}_c &= \boldsymbol{H}_s = 0\end{aligned} \tag{32}$$

Substituting Eqs. (14), (25) and (30) into Eq. (24) gives

$$\boldsymbol{\lambda} = (\boldsymbol{\alpha} + \boldsymbol{\beta}\cos 2\theta + \boldsymbol{\gamma}\sin 2\theta)\mathscr{D} \tag{33}$$

where $\boldsymbol{\alpha}$, $\boldsymbol{\beta}$, and $\boldsymbol{\gamma}$ are computed, for orthotropic damage, from

$$\begin{aligned}\alpha_{mn} &= D\int_{y_D-\bar{y}}^{y_D+\bar{y}}\int_{x_D-\bar{x}}^{x_D+\bar{x}} \left[\left(\frac{1+\nu^2}{1-\nu^2}\right)\frac{\partial^2 W_m}{\partial x^2}\frac{\partial^2 W_n}{\partial x^2} + \left(\frac{2\nu}{1-\nu^2}\right)\left(\frac{\partial^2 W_m}{\partial x^2}\frac{\partial^2 W_n}{\partial y^2} + \frac{\partial^2 W_n}{\partial x^2}\frac{\partial^2 W_m}{\partial y^2}\right) \right. \\ &\quad \left. + \left(\frac{1+\nu^2}{1-\nu^2}\right)\frac{\partial^2 W_m}{\partial y^2}\frac{\partial^2 W_n}{\partial y^2} + \left(\frac{1-\nu}{2(1+\nu)}\right)\frac{\partial^2 W_m}{\partial x\partial y}\frac{\partial^2 W_n}{\partial x\partial y} \right] \mathrm{d}x\,\mathrm{d}y \\ \beta_{mn} &= D\int_{y_D-\bar{y}}^{y_D+\bar{y}}\int_{x_D-\bar{x}}^{x_D+\bar{x}} \left(-\frac{\partial^2 W_m}{\partial x^2}\frac{\partial^2 W_n}{\partial x^2} + \frac{\partial^2 W_m}{\partial y^2}\frac{\partial^2 W_n}{\partial y^2} \right) \mathrm{d}x\,\mathrm{d}y \\ \gamma_{mn} &= -D\int_{y_D-\bar{y}}^{y_D+\bar{y}}\int_{x_D-\bar{x}}^{x_D+\bar{x}} \left(\frac{\partial^2 W_m}{\partial x^2}\frac{\partial^2 W_n}{\partial x\partial y} + \frac{\partial^2 W_n}{\partial x^2}\frac{\partial^2 W_m}{\partial x\partial y} + \frac{\partial^2 W_m}{\partial y^2}\frac{\partial^2 W_n}{\partial x\partial y} + \frac{\partial^2 W_n}{\partial y^2}\frac{\partial^2 W_m}{\partial x\partial y} \right) \mathrm{d}x\,\mathrm{d}y\end{aligned} \tag{34}$$

For the isotropic damage, Eq. (33) becomes identical to that derived in the previous study by Lee et al. (2001): $\boldsymbol{\beta} = \boldsymbol{\gamma} = 0$ and $\boldsymbol{\alpha}$ is computed from

$$\begin{aligned}\alpha_{mn} &= D\int_{y_D-\bar{y}}^{y_D+\bar{y}}\int_{x_D-\bar{x}}^{x_D+\bar{x}} \left[\frac{\partial^2 W_m}{\partial x^2}\frac{\partial^2 W_n}{\partial x^2} + \nu\left(\frac{\partial^2 W_m}{\partial x^2}\frac{\partial^2 W_n}{\partial y^2} + \frac{\partial^2 W_n}{\partial x^2}\frac{\partial^2 W_m}{\partial y^2}\right) + \frac{\partial^2 W_m}{\partial y^2}\frac{\partial^2 W_n}{\partial y^2} \right. \\ &\quad \left. + \left(\frac{1-\nu}{2}\right)\frac{\partial^2 W_m}{\partial x\partial y}\frac{\partial^2 W_n}{\partial x\partial y} \right] \mathrm{d}x\,\mathrm{d}y\end{aligned} \tag{35}$$

Eq. (33) shows that the damage influence matrix $\boldsymbol{\lambda}$ depends on (a) the natural modes of intact plate W_m, (b) the damage orientation θ and (c) the *effective* damage magnitude $\mathscr{D}$ indicating the averaged severity of damage within an SMV.

Eq. (32) or (33) is derived for the plate with a single damage. For the plate with many local damages (say N local damages), it can be readily generalized as follows:

$$\boldsymbol{\lambda} = \sum_{j=1}^{N} (\boldsymbol{\alpha}_j + \boldsymbol{\beta}_j\cos 2\theta_j + \boldsymbol{\gamma}_j\sin 2\theta_j)\mathscr{D}_j \tag{36}$$

where $\mathscr{D}_j$ is the *effective* damage magnitude within the SMV containing the jth damage of orientation θ_j. The SMV containing the jth damage is centered at (x_{Dj}, y_{Dj}) and has the dimensions of $2\bar{x}_j$ and $2\bar{y}_j$ in the x- and y-directions, respectively. The matrices $\boldsymbol{\alpha}_j$, $\boldsymbol{\beta}_j$, and $\boldsymbol{\gamma}_j$ are for the jth damage, all computed from Eq. (34) or (35) by taking the integrals only over the domain from $(x_{Dj} - \bar{x}_j)$ to $(x_{Dj} + \bar{x}_j)$ and from $(y_{Dj} - \bar{y}_j)$ to $(y_{Dj} + \bar{y}_j)$.

Assume a harmonic point force of magnitude F_o is applied at a point $\boldsymbol{x}_F = (x_F, y_F)$. Solving Eq. (21) for $q_m(t)$ and then substituting the solutions into Eq. (18) gives the forced vibration response measured at $\boldsymbol{x}_M = (x, y)$ as follows:

$$w(\boldsymbol{x}_M, t) \cong \left[\sum_{m=1}^{M} \frac{W_m(\boldsymbol{x}_M) W_m(\boldsymbol{x}_F)}{\Omega_m^2 - \omega^2} + \sum_{m=1}^{M} \sum_{n=1}^{M} \lambda_{mn} \frac{W_m(\boldsymbol{x}_M)}{\Omega_m^2 - \omega^2} \frac{W_n(\boldsymbol{x}_F)}{\Omega_n^2 - \omega^2} \right] F_o e^{i\omega t} \tag{37}$$

4. Damage identification theory

4.1. Formulation

It is relatively easy and cheap to use accelerometers to measure the vibration responses of a structure. The vibration signals measured by accelerometers can be processed to compute the FRF. Among several definitions of FRF (Ewins, 1984), the inertance (or accelerance) FRF will be adopted in the present study to develop a new damage identification method. The inertance FRF is defined as the ratio of the acceleration to the applied force.

The inertance FRF measured from a damaged plate can be obtained from Eq. (37) as

$$\mathscr{A}^D(\boldsymbol{x}_M, \omega) = \mathscr{A}(\boldsymbol{x}_M, \omega) + \Delta\mathscr{A}(\boldsymbol{x}_M, \omega) \tag{38}$$

where $\mathscr{A}$ is the inertance FRF measured from the intact plate:

$$\mathscr{A}(\boldsymbol{x}_M, \omega) = -\omega^2 \boldsymbol{\Psi}_M^{\mathrm{T}} \operatorname{diag}[\Omega^2 - \omega^2] \boldsymbol{\Psi}_F \tag{39}$$

and $\Delta\mathscr{A}$ is the perturbed inertance FRF due to the existence of damage

$$\Delta\mathscr{A}(\boldsymbol{x}_M, \omega) = -\omega^2 \boldsymbol{\Psi}_M^{\mathrm{T}} \boldsymbol{\lambda} \boldsymbol{\Psi}_F \tag{40}$$

where

$$\boldsymbol{\Psi}_M = \begin{Bmatrix} \vdots \\ \dfrac{W_m(\boldsymbol{x}_M)}{\Omega_m^2 - \omega^2} \\ \vdots \end{Bmatrix}, \quad \boldsymbol{\Psi}_F = \begin{Bmatrix} \vdots \\ \dfrac{W_m(\boldsymbol{x}_F)}{\Omega_m^2 - \omega^2} \\ \vdots \end{Bmatrix}, \quad \operatorname{diag}[\Omega^2 - \omega^2] = \begin{bmatrix} \ddots & & \\ & \Omega_m^2 - \omega^2 & \\ & & \ddots \end{bmatrix} \tag{41}$$

From Eq. (38), one may see that the effects of damage appear only in the perturbed inertance FRF ($\Delta\mathscr{A}$) through the damage influence matrix $\boldsymbol{\lambda}$ given by Eq. (36).

Substituting Eq. (36) into Eq. (40) gives

$$\sum_{j=1}^{N} \left[a_j(\boldsymbol{x}_M, \omega) + b_j(\boldsymbol{x}_M, \omega) \cos 2\theta_j + c_j(\boldsymbol{x}_M, \omega) \sin 2\theta_j \right] \mathscr{D}_j = \Delta\mathscr{A}(\boldsymbol{x}_M, \omega) \tag{42}$$

where

$$\begin{aligned} a_j(\boldsymbol{x}_M, \omega) &= -\omega^2 \boldsymbol{\Psi}_M^{\mathrm{T}}(\boldsymbol{x}_M, \omega) \boldsymbol{\alpha}_j \boldsymbol{\Psi}_F(\omega) \\ b_j(\boldsymbol{x}_M, \omega) &= -\omega^2 \boldsymbol{\Psi}_M^{\mathrm{T}}(\boldsymbol{x}_M, \omega) \boldsymbol{\beta}_j \boldsymbol{\Psi}_F(\omega) \\ c_j(\boldsymbol{x}_M, \omega) &= -\omega^2 \boldsymbol{\Psi}_M^{\mathrm{T}}(\boldsymbol{x}_M, \omega) \boldsymbol{\gamma}_j \boldsymbol{\Psi}_F(\omega) \end{aligned} \tag{43}$$

Eq. (42) shows the relationship between the damage information (i.e., effective damage magnitudes $\mathscr{D}_j$ and damage orientations θ_j) and the damage-induced change in dynamic response (i.e., the perturbed inertance FRF $\Delta\mathscr{A}$). Thus, once $\Delta\mathscr{A}$ is experimentally measured from the damaged plate, Eq. (42) can be used to identify the unknown damage information.

For a chosen set of $(\boldsymbol{x}_M, \omega)$, Eq. (42) provides an algebraic equation for unknown effective damage magnitudes $\mathscr{D}_j$ and damage orientations θ_j. Thus, by properly choosing as many different sets of $(\boldsymbol{x}_M, \omega)$ as required, say N for instance, and denoting the ith set of $(\boldsymbol{x}_M, \omega)$, by the subscript i, a set of simultaneous algebraic equations can be obtained in the form as

$$\boldsymbol{X}(\boldsymbol{\Theta})\boldsymbol{\mathscr{D}} = \Delta\boldsymbol{\mathscr{A}} \tag{44}$$

where

$$\begin{aligned}
\boldsymbol{\mathscr{D}} &= \{\, \mathscr{D}_1 \quad \mathscr{D}_2 \quad \cdots \quad \mathscr{D}_N \,\}^{\mathrm{T}} \\
\boldsymbol{\Theta} &= \{\, \theta_1 \quad \theta_2 \quad \cdots \quad \theta_N \,\}^{\mathrm{T}} \\
\Delta\boldsymbol{\mathscr{A}} &= \{\, \Delta\mathscr{A}_1 \quad \Delta\mathscr{A}_2 \quad \cdots \quad \Delta\mathscr{A}_N \,\}^{\mathrm{T}}
\end{aligned} \tag{45}$$

and

$$\begin{aligned}
&\boldsymbol{X}(\boldsymbol{\Theta}) = \boldsymbol{A} + \boldsymbol{B}\,\mathrm{diag}[\cos 2\theta] + \boldsymbol{C}\,\mathrm{diag}[\sin 2\theta] \\
&\boldsymbol{A} = [a_{ij}] = a_j(\boldsymbol{x}_M, \omega)_i \\
&\boldsymbol{B} = [b_{ij}] = b_j(\boldsymbol{x}_M, \omega)_i \quad (i, j = 1, 2, \ldots, N) \\
&\boldsymbol{C} = [c_{ij}] = c_j(\boldsymbol{x}_M, \omega)_i \\
&\mathrm{diag}[\cos 2\theta] = \begin{bmatrix} \ddots & & \\ & \cos 2\theta_j & \\ & & \ddots \end{bmatrix} \\
&\mathrm{diag}[\sin 2\theta] = \begin{bmatrix} \ddots & & \\ & \sin 2\theta_j & \\ & & \ddots \end{bmatrix}
\end{aligned} \tag{46}$$

Eqs. (44) represent the damage identification theory developed in this paper for locating many local line crack-like damages and also for identifying their severities (i.e., effective damage magnitudes) and orientations with respect to the reference coordinates.

For the problems with isotropic damages, the matrices $\boldsymbol{B}$ and $\boldsymbol{C}$ should vanish and Eqs. (44) are reduced to the theory developed in the previous study (Lee et al., 2001), that is

$$\boldsymbol{A}\boldsymbol{\mathscr{D}} = \Delta\boldsymbol{\mathscr{A}} \tag{47}$$

For isotropic damage, the matrix $\boldsymbol{A}$ is computed from Eq. (43a) by using the matrix $\boldsymbol{\alpha}$ defined by Eq. (35). By properly choosing N different sets of $(\boldsymbol{x}_M, \omega)$, the number of simultaneous algebraic equations can be made equal to that of SMVs (or the number of unknown $\mathscr{D}_j$). Then, one can apply the direct matrix inversion method to solve Eqs. (47) for $\boldsymbol{\mathscr{D}}$.

4.2. Computation: iterative method

Eq. (44) is nonlinear with respect to the damage orientation $\boldsymbol{\Theta}$, which are coupled with effective damage magnitude $\mathscr{D}$. Thus, the iterative solution technique is inevitable for identifying orthotropic damages.

Once $\Delta\mathscr{A}$ is given (i.e., measured), the relationship between the perturbations (or errors) in $\mathscr{D}$ and $\boldsymbol{\Theta}$ can be derived from Eq. (44) as follows:

$$\Delta\mathscr{D} = [2\boldsymbol{X}^{-1}(\Theta)\boldsymbol{Y}(\Theta)\,\mathrm{diag}[\mathscr{D}_j]]\Delta\boldsymbol{\Theta} \equiv \boldsymbol{S}\Delta\boldsymbol{\Theta} \tag{48}$$

or

$$\Delta\boldsymbol{\Theta} = \boldsymbol{S}^{-1}\Delta\mathscr{D} \tag{49}$$

where

$$\begin{aligned} &\boldsymbol{Y}\ (\Theta) = \boldsymbol{B}\,\mathrm{diag}[\sin 2\theta] - \boldsymbol{C}\,\mathrm{diag}[\cos 2\theta] \\ &\Delta\boldsymbol{\Theta} = \{\,\Delta\theta_1 \quad \Delta\theta_2 \quad \cdots \quad \Delta\theta_N\,\}^{\mathrm{T}} \end{aligned} \tag{50}$$

The matrix $\boldsymbol{S}$ in Eq. (48) indicates the sensitivity of $\mathscr{D}$ to the perturbation in $\boldsymbol{\Theta}$, while the matrix $\boldsymbol{S}^{-1}$ in Eq. (49) indicates the sensitivity of $\boldsymbol{\Theta}$ to the perturbation in $\mathscr{D}$. For numerical illustration, the matrices $\boldsymbol{S}$ and $\boldsymbol{S}^{-1}$ are given in Fig. 2 for the plate with a local damage shown in Fig. 6(a). It is very clear from Fig. 2 that $\mathscr{D}$ is not so sensitive to the perturbation in $\boldsymbol{\Theta}$, while $\boldsymbol{\Theta}$ is extremely sensitive to the perturbation in $\mathscr{D}$. Thus, when applying an iterative solution method to Eqs. (44), it is not desirable to update $\boldsymbol{\Theta}$ by directly using the perturbation in $\mathscr{D}$. From this observation, an iterative method shown in Fig. 3 is used in this study. The procedure of the present iterative solution method is further detailed in the following:

(1) First guess the initial value $\boldsymbol{\Theta}(1)$ and then compute the corresponding initial value $\mathscr{D}(1)$ from Eqs. (44) by the direct use of matrix inversion.
(2) Substitute the initial value $\mathscr{D}(1)$ into Eqs. (44) and compute the updated value of $\boldsymbol{\Theta}$ by applying the Newton–Raphson method to solve the nonlinear algebraic equations in $\boldsymbol{\Theta}$.
(3) Compute the increment $\Delta\boldsymbol{\Theta}$ by subtracting the previous value of $\boldsymbol{\Theta}$ from the updated value of $\boldsymbol{\Theta}$ and then use the results to compute the increment $\Delta\mathscr{D}$ from Eq. (48).
(4) Compute the updated value of $\mathscr{D}$ by adding $\Delta\mathscr{D}$ to its previous value.
(5) Go back to (2), and use the updated value of $\mathscr{D}$ as the new initial value to start the next iteration.

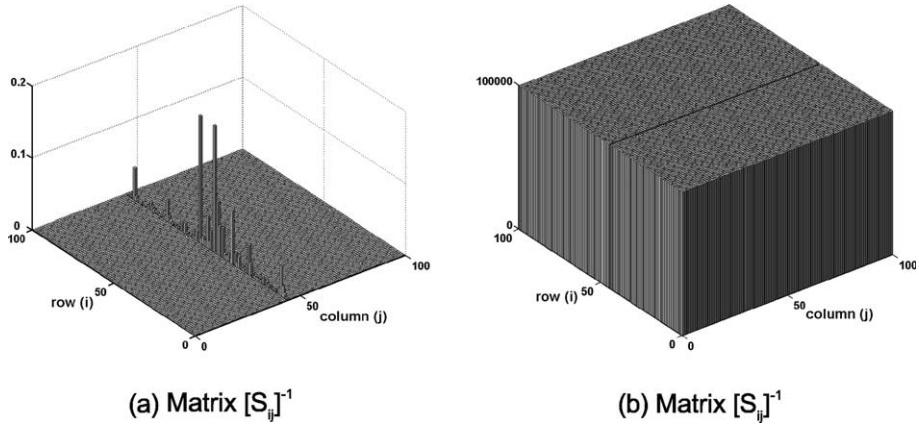

Fig. 2. (a) The matrix $\boldsymbol{S}$ in Eq. (48) and (b) its inverse matrix $\boldsymbol{S}^{-1}$ in Eq. (49).

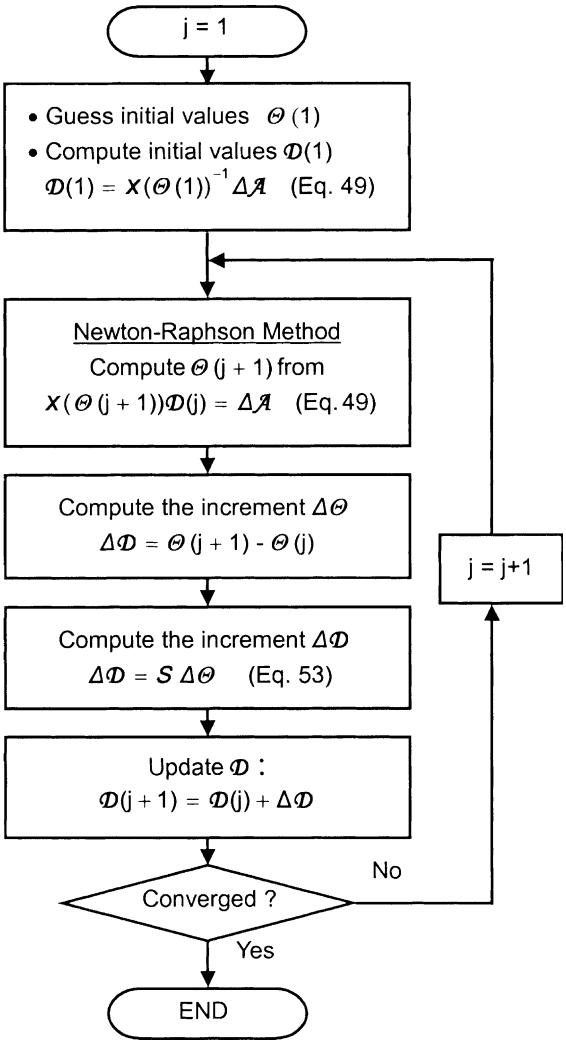

Fig. 3. Iterative solution method used in the present study.

(6) Repeat the iteration process (from (2) to (5)) until $\mathscr{D}$ and $\boldsymbol{\Theta}$ are converged to certain values, within a pre-specified accuracy limit.

5. Numerical illustrations and discussions

First, the effects of damage orientation on the vibration responses of a plate with a line crack are investigated. Fig. 4 shows the example plate, which is simply supported. The geometric and material properties are: thickness $h = 0.004$ m, sizes $L_x = L_y = L = 0.5$ m, Young's modulus $E = 72$ GPa, Poisson's ratio $v = 0.33$, and mass density 2800 kg/m^3. The line crack is 0.032 m long and is located at the center of plate. A point harmonic force (excitation frequency $\omega = 100$ Hz) is applied at the middle of the plate. To compute

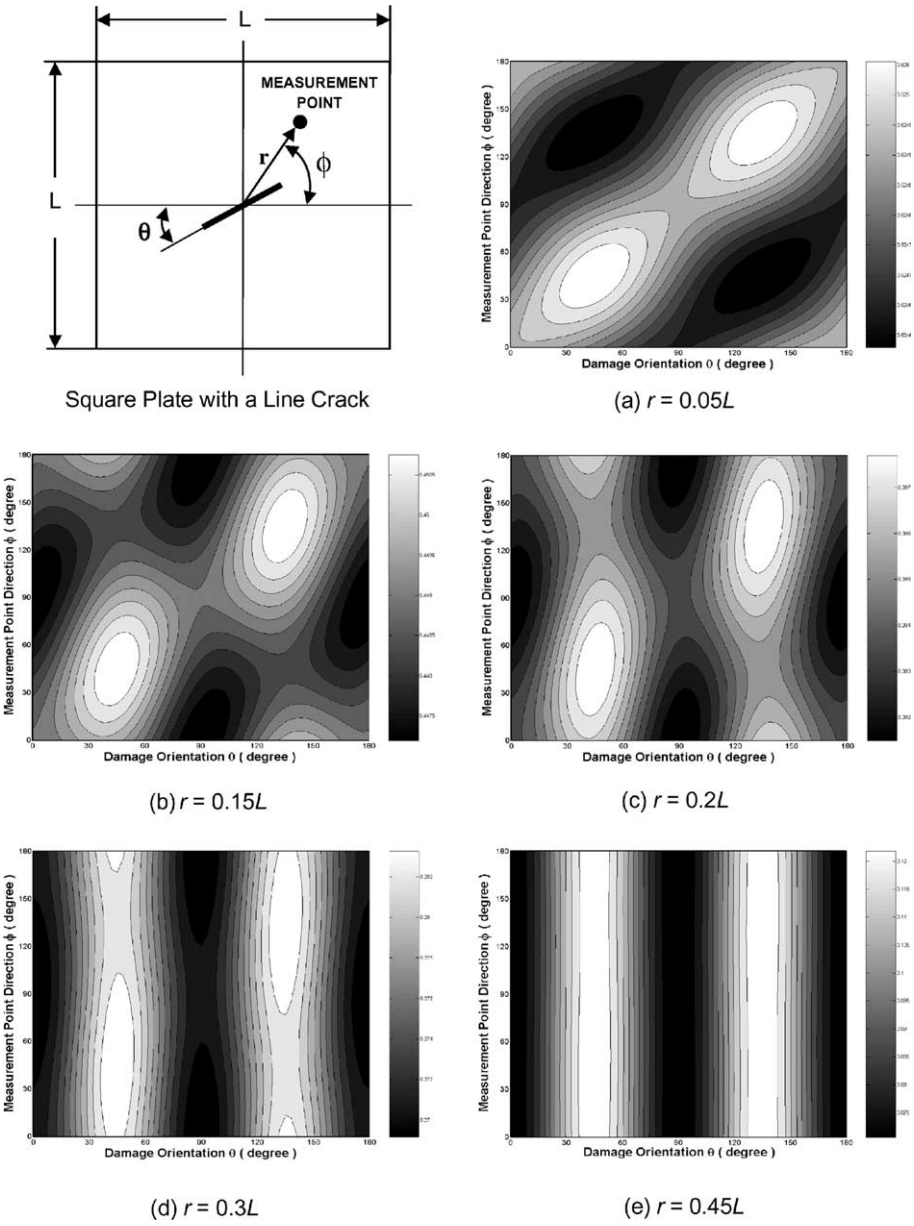

Fig. 4. Non-dimensional vibration amplitudes of a square plate measured at different distances from the line crack (r) with varying the crack orientation (θ) and the angle of measurement point direction (ϕ).

the effective elastic stiffnesses Q_{ij}^{D} for damage zone (i.e., SMV), the dimensions of the SMV are chosen as $2\bar{x} = 2\bar{y} = 0.04$ m so that the effective damage magnitude becomes $\mathscr{D} = 0.5$.

Comparing with the natural frequencies of the intact plate and the plate with isotropic damage, Table 1 shows the change in the natural frequencies of the plate with orthotropic damage with varying the orientation of damage. One may see from Table 1 that, in general, the natural frequencies are reduced in

Table 1
Damage information pre-specified for damage identification tests

Example problems	Effective damage magnitude	Damage orientation (degrees)	Damage location $(x_D m, y_D m)$	Dimensions of finite segment $(2\bar{x}m, 2\bar{y}m)$
One damage	$\mathscr{D} = 0.5$	$\theta = 45$	(0.225, 0.225)	(0.05, 0.05)
Three damages	$\mathscr{D}_1 = 0.3$	$\theta_1 = 0$	(0.125, 0.375)	(0.05, 0.05)
	$\mathscr{D}_2 = 0.7$	$\theta_2 = 45$	(0.275, 0.075)	(0.05, 0.05)
	$\mathscr{D}_3 = 0.5$	$\theta_3 = 30$	(0.275, 0.275)	(0.05, 0.05)

magnitude due to the presence of damage and they are dependent of damage direction. The geometric symmetry of the example square plate will be destroyed by the orthotropic damage, while not by the isotropic damage. Thus, as expected, Table 1 shows that the natural frequency for mode (1,2) is different from that for mode (2,1) for the case of orthotropic damage, while they are the same for the case of isotropic damage. Fig. 4 shows the vibration amplitudes of a square plate measured at different distances from the crack (r) with varying the crack orientation (θ) and the measurement point direction (ϕ). One may observe that, as the distance of the measurement point from the crack gets larger and larger, the effects of the measurement point direction disappear and only the effects of crack orientation become dominant.

Next, the numerically simulated damage identification tests are conducted to validate the present SDIM. Two example problems shown in Fig. 5 are considered: (a) the plate with a line crack-like damage (single damage problem), and (b) the plate with three line crack-like damages (three damages problem). The two plates have the simply supported boundary conditions, and they have the same dimensions and material properties: thickness $h = 4$ mm, $L_x = L_y = 0.5$ m, Young's modulus $E = 72$ GPa, Poisson's ratio $\nu = 0.33$, and mass density 2800 kg/m^3. The details of the line crack-like damages considered for two example problems are given in Table 2. As shown in Fig. 5, the plates are divided into 100 equal-sized finite segments, and the damage identification analysis are conducted to determine the effective damage magnitudes and orientations within all finite segments. A point harmonic force (excitation frequency $\omega = 100$ Hz) is applied at the middle points of plates, and the inertance FRF is simulated from Eq. (38) at each center of finite segments.

To measure the accuracy of the identified effective damage magnitudes with respect to true ones (i.e., pre-specified values), a root mean squared 'damage identification error (DIE)' defined by

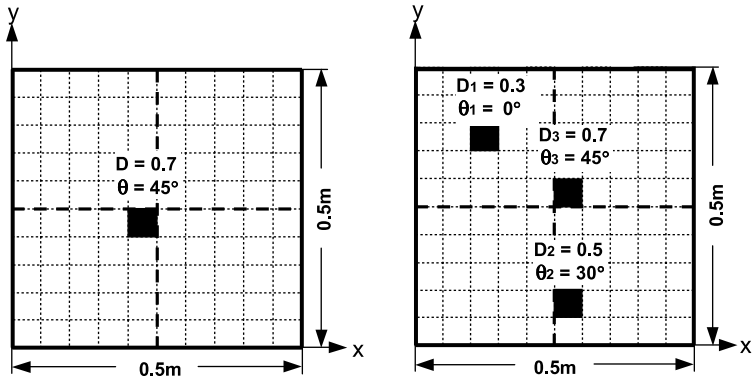

Fig. 5. Two example problems considered for numerically simulated damage identification tests.

Table 2
The change in natural frequencies (Hz) of the plate shown in Fig. 4

Modes	Intact	Isotropic damage	Orthotropic damage			
			$\theta = 0°$	$\theta = 15°$	$\theta = 30°$	$\theta = 45°$
1st (1,1)	77.95	76.30	75.03	74.86	74.46	74.23
2nd (1,2)	194.87	194.23	192.91	192.75	192.40	192.20
3rd (2,1)	194.87	194.23	194.50	194.52	194.56	194.58
5th (1,3)	389.74	377.32	364.94	365.46	366.49	367.01
10th (1,4)	662.56	654.56	660.11	658.97	656.01	653.90
20th (4,4)	1247.16	1241.80	1239.18	1232.93	1219.88	1212.97
30th (3,6)	1753.82	1734.85	1742.71	1742.61	1742.40	1742.31

$$\mathrm{DIE} = \sqrt{\frac{1}{L_x L_y}\sum_{j=1}^{N_{\mathrm{seg}}} 4\bar{x}_j\bar{y}_j\left(D_j^{\mathrm{T}} - D_j^{I}\right)^2} \tag{51}$$

is used herein. The superscripts T and I indicate the 'true' and 'identified' values, respectively. N_{seg} is the number of finite segments, and the subscript j indicates the quantities for the jth finite segment. As the value of DIE gets smaller, the identified effective damage magnitudes get closer to the true values.

Figs. 6 and 7 show the damage identification results for the single damage problem and three damages problem, respectively, all obtained without taking into account the measurement noise in FRF. One may see from Figs. 6 and 7 that, as the iteration is repeated, the damage identification results obtained by the present SDIM indeed converge to the true values. To obtain very accurate damage identification results, within 0.5% errors for both the effective damage magnitudes and damage orientation, Figs. 6 and 7 show that total 20 iterations and total 40 iterations are required for the present single damage problem and three damages problem, respectively.

In practice, the experimentally measured inertance FRF is liable to be contaminated by the measurement noise. The measurement noise may be lowered below about 5–7% by most well prepared vibration tests (Lee and Shin, 2002b). To investigate the effects of measurement noise in FRF on the reliability of the present SDIM, e% random noise is added to the simulated inertance FRF by following the approach by Thyagarajan et al. (1998):

$$\overline{\mathscr{A}} = \mathscr{A}\left(1 + \frac{e}{100} \times \mathrm{randn}\right) \tag{52}$$

where $\overline{\mathscr{A}}$ is the inertance FRF contaminated by e% random noise, and randn is the random noise generator function in MATLAB®.

The effects of the noise in FRF on the damage identification results are shown in Fig. 8 for the single damage problem and in Fig. 9 for the three damages problem. The results shown in Figs. 8 and 9 are obtained from the mean values of ten simulations. For each simulation, total 20 iterations are conducted for the single damage problem, and total 40 iterations for the three damages problem. As expected, as the level of random noise in FRF is increased, the larger level of incorrect effective damage magnitude appears at damage-free finite segments, increasing the value of DIE. Figs. 8 and 9 show that the present SDIM identifies the location and effective damage magnitude of the damaged finite segments quite accurately, within about 5% errors, as far as the noise in FRF is kept below about 10% for one damage problem and about 7% for three damages problem. In addition, Figs. 8 and 9 show that the present SDIM can fairly well identify the damage orientation at damaged finite segments, which is the unique and important feature of the present theory. From Figs. 8 and 9, one may observe that, when compared with the location and severity of damage, the damage orientation is more sensitive to the random noise in FRF. To predict the

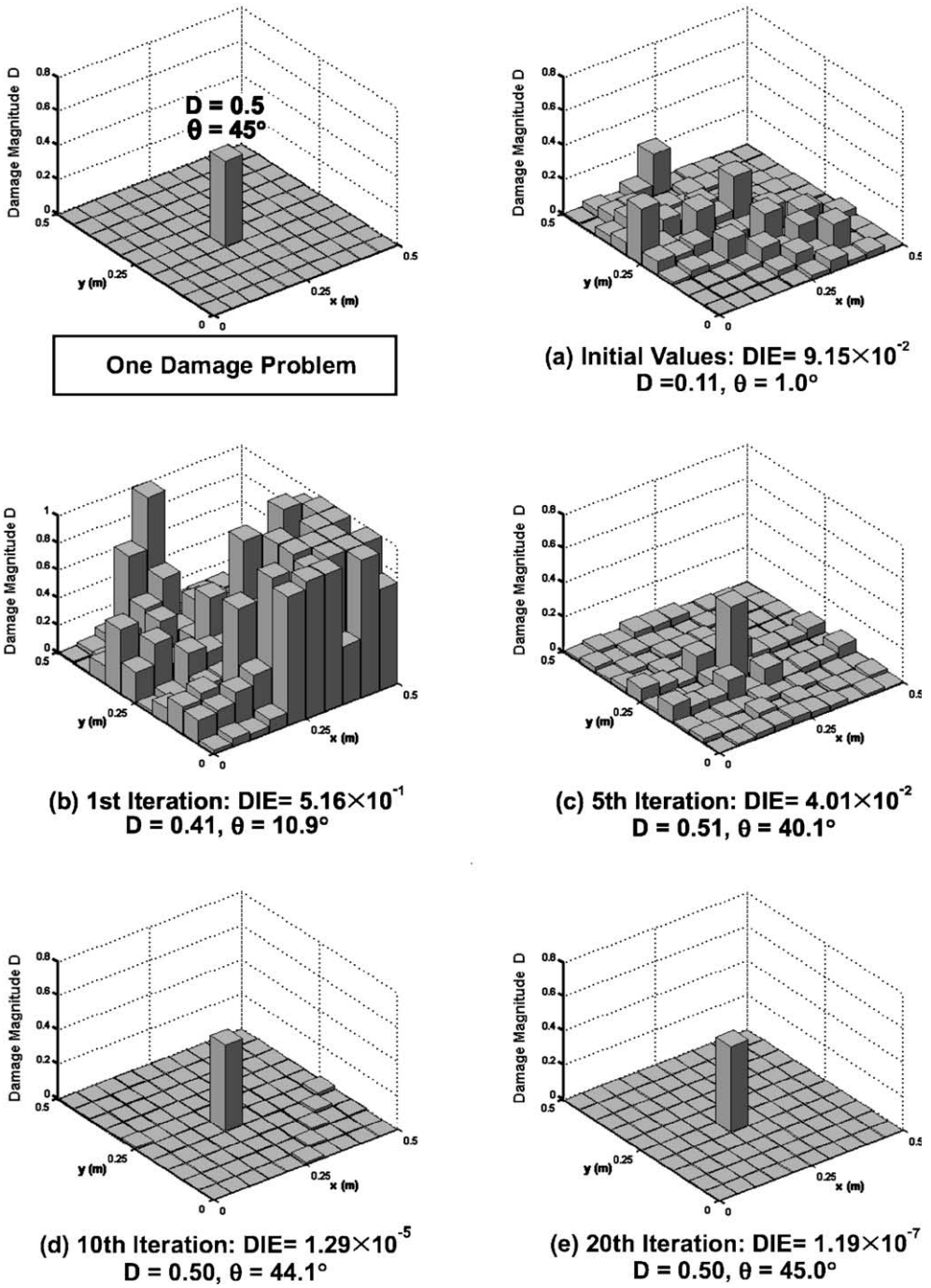

Fig. 6. Damage identification results for the one damage problem, without considering the effects of measurement noise in FRF.

damage orientation within about 5% errors, Figs. 8 and 9 show that the noise in FRF should be below about 7% for one damage problem and about 5% for three damages problem. Thus, in general, identifying

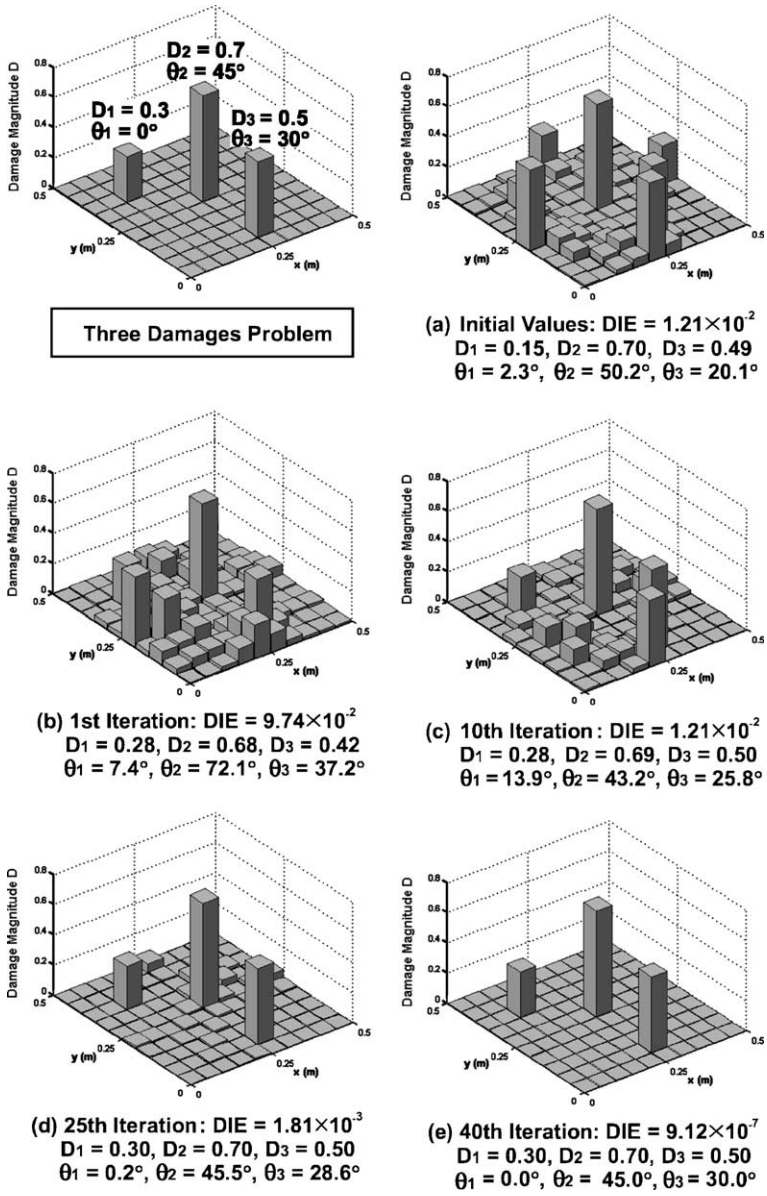

Fig. 7. Damage identification results for the three damages problem, without considering the effects of measurement noise in FRF.

damage orientation seems to require more carefully prepared FRF-measurement tests in order to lower the level of measurement noise below than that required for identifying damage location and magnitudes only.

6. Conclusions

In the present paper, first, the equation of motion of the thin uniform plate with crack-like local damages is derived. Based on a theory of continuum damage mechanics, a local damage is represented in terms of

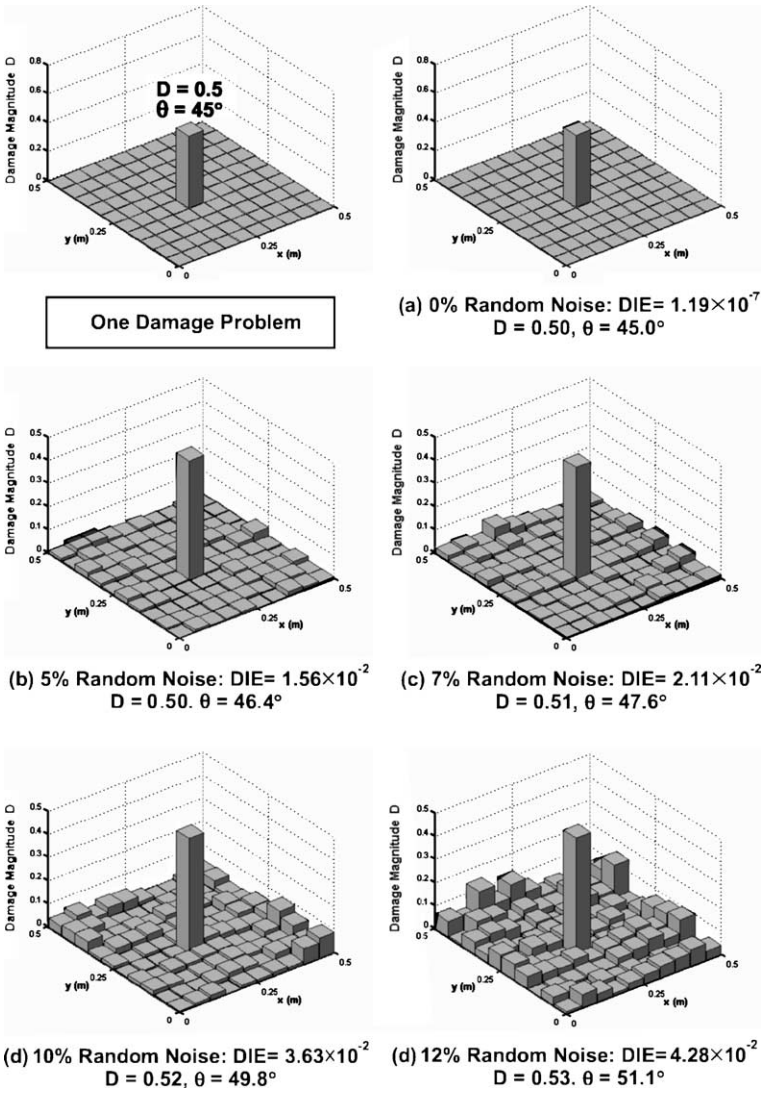

Fig. 8. The effects of measurement noise in FRF on the damage identification results for the three damages problem.

the effective orthotropic elastic stiffnesses. A new damage identification theory is then formulated from the forced vibration response of a damaged plate. The present damage identification theory has the capability of identifying the locations, severities, and orientations of local damages, all together at a time. Numerical investigation is given to the effects of damage orientation on the vibration response of a simply supported square plate. To validate the present damage identification theory, the numerically simulated damage identification tests are conducted by taking into account the measurement noises in FRFs. The numerical tests show that, up to about 7% random noises in FRF, the present damage identification theory can fairly well identify the locations, severities, and orientations of all damages considered in the present study.

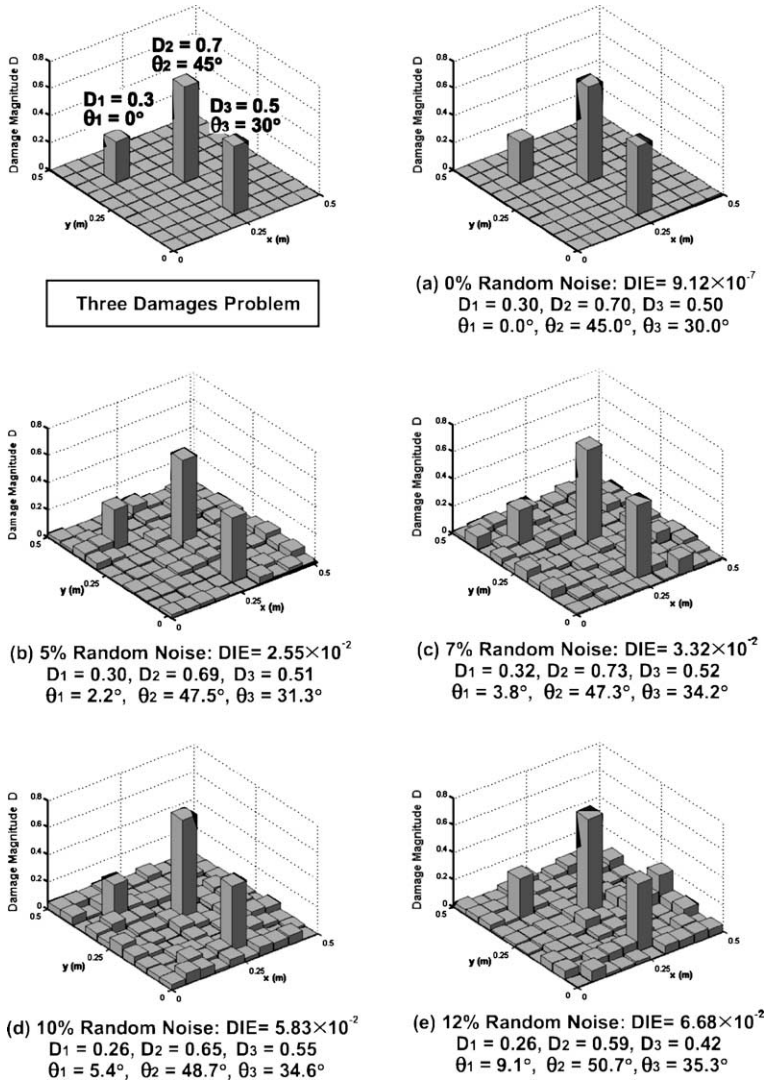

Fig. 9. The effects of the measurement noise in FRF on the damage identification results for the one damage problem.

Acknowledgement

This work was supported by Grant No. R01-2000-00295-0 from the Korea Science and Engineering Foundation.

References

Adams, R.D., Cawley, P., Pye, C.J., Stone, B.J., 1978. A vibration technique for non-destructively assessing the integrity of structures. Journal of Mechanical Engineering Science 20 (2), 93–100.

Araujo dos Santos, J.V., Mota Soares, C.M., Mota Soares, C.A., Pina, H.L.G., 2000. A damage identification: numerical model based on the sensitivity of orthogonality conditions and least squares techniques. Computers and Structures 78, 283–291.

Bicanic, N., Chen, H.P., 1997. Damage identification in framed structures using natural frequencies. International Journal of Numerical Methods in Engineering 40, 4451–4468.
Castello, D.A., Stutz, L.T., Rochinha, F.A., 2002. A structural defect identification approach based on a continuum damage model. Computers and Structures 80, 417–436.
Cawley, P., 1984. The impedance method of non-destructive inspection. Journal of NDT International 17, 59–65.
Cawley, P., Adams, R.D., 1979. The location of defects in structures from measurements of natural frequencies. Journal of Strain Analysis 14 (2), 49–57.
Chen, H.P., Bicanic, N., 2000. Assessment of damage in continuum structures based on incomplete modal information. Computers and Structures 74, 559–570.
Cornwell, P., Doebling, S.W., Farrar, C.R., 1999. Application of the strain energy damage detection method to plate-like structures. Journal of Sound and Vibration 224 (2), 359–374.
Dimarogonas, A.D., 1996. Vibration of cracked structures: a state of the art review. Engineering Fracture Mechanics 55 (5), 831–857.
Ewins, D.J., 1984. Modal Testing: Theory and Practice. Research Studies Press, New York.
Hassiotis, S., 2000. Identification of damage using natural frequencies and Markov parameters. Computers and Structures 74, 365–373.
Kabe, A.M., 1985. Stiffness matrix adjustment using mode data. AIAA Journal 28 (9), 1431–1436.
Khadem, S.E., Rezaee, M., 2000. An analytical approach for obtaining the location and depth of an all-over part-through crack on externally in-plane loaded rectangular plate using vibration analysis. Journal of Sound and Vibration 230 (2), 291–308.
Lee, H.P., Lim, S.P., 1993. Vibration of cracked rectangular plates including transverse shear deformation and rotary inertia. Computers and Structures 49, 715–718.
Lee, U., Kim, N., 2001. Dynamics of damaged plates. In: 42nd AIAA Structures, Structural Dynamics and Materials Conference, AIAA-2001-1391.
Lee, U., Kim, N., Shin, J., 2001. Identification of damages within a plate structure. In: 42nd AIAA Structures, Structural Dynamics and Materials Conference, AIAA-2001-1244.
Lee, U., Lesieutre, G.A., Fang, L., 1997. Anisotropic damage mechanics based on strain energy equivalence and equivalent elliptical microcracks. International Journal of Solids and Structures 34 (33/34), 4377–4397.
Lee, U., Shin, J., 2002a. An frequency response function-based structural damage identification method. Computers and Structures 80 (2), 117–132.
Lee, U., Shin, J., 2002b. A frequency-domain method of structural damage identification formulated from the dynamic stiffness equation of motion. Journal of Sound and Vibration 257 (4), 615–634.
Lew, J.S., 1995. Using transfer function parameter changes for damage detection of structures. AIAA Journal 33 (11), 2189–2193.
Lim, T.W., 1995. Structural damage detection using constrained eigenstructure assignment. AIAA Journal of Guidance Control and Dynamics 18 (3), 411–418.
Luo, H., Hanagud, S., 1997. An integral equation for changes in the structural dynamics characteristics of damaged structures. International Journal of Solids and Structures 34 (35/36), 4557–4579.
Lynn, P.P., Kumbasar, N., 1967. Free vibrations of thin rectangular plates having narrow cracks with simply supported edges. Development in Mechanics 4, 911–928.
Pandey, A.K., Biswas, M., 1995. Damage diagnosis of truss structures by estimation of flexibility change. International Journal of Analytical and Experimental Modal Analysis 10 (2), 104–117.
Reddy, J.N., 1999. Theory and Analysis of Elastic Plates. Taylors & Francis, Philadelphia.
Ricles, J.M., Kosmatka, J.B., 1992. Damage detection in elastic structures using vibratory residual forces and weighted sensitivity. AIAA Journal 30 (9), 2310–2316.
Thyagarajan, S.K., Schulz, M.J., Pai, P.F., 1998. Detecting structural damage using frequency response functions. Journal of Sound and Vibration 210 (1), 162–170.
Wang, Z., Lin, R.M., Lim, M.K., 1997. Structural damage detection using measured FRF data. Computer Methods in Applied Mechanics in Engineering 147, 187–197.
Whitney, J.M., 1996. Structural Analysis of Laminated Anisotropic Plates. Technomic Publishing, Lancaster.
Zimmermann, D.C., Kaouk, M., 1994. Structural damage detection using a minimum rank update theory. ASME Journal of Vibration and Acoustics 116, 222–231.